



The Effects of Strain on Stability of Passivation in Austenitic Stainless Steels: Comparison with Heat Treatment

N. Srinivasan¹ · S.S. Kumaran¹

Received: 28 August 2018 / Accepted: 28 December 2020 / Published online: 20 January 2021
© The Society for Experimental Mechanics, Inc 2021

Abstract

The passive film mainly consists of oxides and hydroxide and is a key for corrosion protection of metallic materials. It increases the durability and performance of engineering components by spontaneous formation of effective, adherent barrier between the corrosive environment and a substrate. Herein, influence of plastic strain and after heat treatment on austenitic stainless steels was compared with the focus on stability of the passive film. The following materials were used in this study: Sanicro 28™, AISI 316 L, and AISI 304 L. These specimens were subjected to a true strain of 0.58. The conventional three-electrode cell was used to record the anodic potentiodynamic polarization curves. The grain size and other misorientation parameters were extracted using electron backscattered diffraction (EBSD). Fourier transform infrared spectroscopy (FTIR)-imaging was used for capturing chromium oxide (Cr_2O_3) peaks for all specimens. The average area of Cr_2O_3 peaks was compared with deformed and after heat treatment of 700 °C 30 min specimens. It was found that heat-treated specimens exhibited slightly higher average area of Cr_2O_3 than deformed.

Keywords Austenitic stainless steels · Passivity · Effect of strain · Heat treatment · Electron backscattered diffraction (EBSD) · Fourier transformed infrared spectroscopy (FTIR)-imaging

Introduction

Austenitic stainless steels of 18% chromium and 8% nickel are potentially used in harsh engineering applications due to their good mechanical and corrosion properties, particularly at elevated temperatures. The formation of precipitation and their influence on properties have been studied in detail by researchers across the globe [1, 2]. It has been reported that the exposure to elevated temperature range (500 °C–800 °C), leads to precipitation of M_{23}C_6 type of carbides [3]. In general these precipitates form at grain boundaries that decrease corrosion resistance. The improper heat treatment, welding, during service of austenitic stainless steels increase the risk of

precipitation, particularly M_{23}C_6 carbides, thereby forming chromium depletion zone, adjacent to carbides. Further, it has been shown that chromium depletion zone at/along the grain boundaries is clear indication of materials susceptibility to intergranular corrosion (IGC). There has been mitigation techniques/strategies available for sensitization of stainless steel [4, 5]. During fabrication of austenitic stainless steel components, the plastic strain is generated [6, 7]. The factors such as deformation, microstructure, grain size [8], alloy chemistry [9], condition the corrosion behavior. Further, it is known that contradictions exist about the exact role of the deformation despite several studies have been carried out by the researchers. In addition, all the reports were concluded based on the combined effect. It has been reported that 23% deformation of austenitic stainless steels exhibited increased corrosion resistance [10]. Controlling and enhancing the corrosion resistance of metallic materials remains critical. This requires an understanding of substructural features/parameters. The ‘self-cleaning’ tendency in austenitic stainless steel is attractive and plays key role in determining corrosion resistance. The corundum type chromium oxide (Cr_2O_3) plays a major role in the

✉ N. Srinivasan
srinivasan.narayanan@vit.ac.in

S.S. Kumaran
senthilkumaran.s@vit.ac.in

¹ Department of Manufacturing Engineering, School of Mechanical Engineering, VIT, Vellore Institute of Technology, Tamil Nadu 632014 Vellore, India



passivating of stainless steel [11]. The science behind the long-lasting shining of stainless steel is passivity. In general, the passivity is defined as materials ability of corrosion resistance when the thermodynamic tendency favors a corrosion reaction. It is also said that, ease of surface barrier film of oxide /hydroxide. Further the passive film is usually of semiconducting oxide (oxide /hydroxide) layer of n or p-type semiconductor properties. The loss of passivity leading pitting corrosion is generally explained by the three main mechanisms. These are penetration, film breaking, and adsorption. The alloy chemistry [12–14], thermal history and microstructure [15] and test environment (exposure) affect the stability of passive film. For instance, the niobium (Nb) is generally added to stabilize the austenitic steel grades thereby increase the resistance of IGC and pitting corrosion [12, 13]. Further, nitrogen (N), nickel (Ni) are also added for stabilizing austenite. The microstructure includes, grain, grain boundary, inclusion, precipitates, grain orientation, nature of grain boundary and its types have also been shown to affect the passivation. It is widely known that halides and chlorides is detrimental to stability of passive film and it leads to initiation of pitting corrosion. It is also reported that the addition of chlorides [16], produced defective passive films [17], further, the role of chromium (Cr), in determining the defect densities of passive film is high. They have reported that less defective passive film for stainless steel specimens with higher Cr [17]. The direct observation of passive film was observed using advanced TEM techniques. They reported that the passive film formed on duplex stainless steels exhibited step-like unevenness [18]. Thus the passive film is influenced by the composition and microstructures of steel substrate. Although, the passive film of stainless steel is much discussed and widely explored, the exact relationship between the influence of local microstructure and the stability of passive film and initiation of pits is not understood. In another study, the local electrical resistance of the surface passive film has been studied by the researchers using conductive atomic force microscopy (CAFM) [19]. It has been reported that increase in corrosion resistance of ultrafine-grained +annealed duplex stainless steels in borate buffer test solution [20]. The same research group indicated reverse trend, deteriorated corrosion resistance of ultrafine-grained +annealed specimens in a 0.1 M NaCl test solutions, further in 0.5 M H₂SO₄ and borate buffer solution, it is reported that increase in corrosion resistance of passive film reverses [21]. The interrupted tensile test was carried out for studying passivity of 316 L stainless steel [22]. They found that due to increased cation vacancy reduced corrosion resistance of passive film. The stoichiometry, microstructure and electronic properties of passive film strongly condition the stability of

passive film. Since the stability of passive film is critical for engineering applications. Hence researchers have been extensively studied passive film using spectroscopy and microscopy techniques. These are Auger electron spectroscopy (AES) and x-ray photoelectron spectroscopy (XPS) and Mott-Schottky analysis. It is reported that the doping concentration in passive film, increased the defect density (through the application of in-situ tensile strain in AISI 316 L stainless steels) in passive film [22, 23]. Further, when deformed AISI 304 stainless steel is unloaded, the more quantity of strain-induced martensite form, this tendency is very high as reported. This behavior is observed during cyclic loading. It is reported that, the deformed specimens of stainless steels exhibited more chromium content than the heat treated [24]. However Rangel et al. reported that opposite [25]. This was the motivation in this study. Herein, influence of plastic strain and after heat treatment on austenitic stainless steels were compared with the focus on stability of passive film. The stability of passive film was related to the intensity of Cr₂O₃ as measured from Fourier transform infrared spectroscopy (FTIR)-imaging. In general, spectroscopy deals with interaction between matter and light. The infrared (IR) spectroscopy is a technique of using electromagnetic radiation in infrared region. Thus, IR spectroscopy is the analysis (absorption, emission and reflection) of infrared light interacting with molecule. The included IR regions are approximately classified into near, mid and far infrared. The FTIR-imaging uses the Fourier series transform (a mathematical concept, named after a French mathematician and physicist called Joseph Fourier) that converts data into spectrum to reveal very fundamental information about the molecular structure. The infrared light from the source is allowed to pass through the Michelson interferometer, refracted and transmitted forming an interferogram, converted into a spectrum by Fourier transform. Spectroscopy, in general, non-destructive method of determining the atomic or molecular structure. When the infrared radiation interacts with a substance, the following is possible: absorption, transmission, reflection, and scattering. These provide ample information about the structure and the energy level. The very detailed piece of information about the mechanism and working principle are found in this reference [26]. The possibilities of using FTIR spectroscopy are enormous and increasing. The major application includes (i) compound identification, (ii) structural identification, (iii) quantitative analysis of species and (iv) measuring fundamental properties, and (v) characterization of chemical structure of molecules, and other species. The technological advancement and new possibilities of combining microscopic and spectroscopic add/improve new insights to fundamental understandings for closer inspection. It is reported that the passivity

Table 1 Chemical composition of types of austenitic stainless steels used in this study (wt%)

	C	P	Mn	S	Cr	Mo	Si	Ni	Cu	N
Sanicro 28™	0.020	0.025	2.0	0.015	27.00	3.6	0.60	31.0	1.09	–
AISI 316 L	0.020	0.010	1.0	0.020	16.25	2.3	0.38	10.73	–	0.10
AISI 304 L	0.029	0.025	1.78	0.010	18.01	–	0.20	8.21	–	0.037

exhibit extreme heterogeneities at the micro/nano scale. The role of passive film was extensively studied using AFM and XPS techniques [27]. The volta potential parameter from scanning Kelvin probe force microscopy (SKPFM) has been used to study about passive film of duplex stainless steel [28]. SKPFM is a combination of Kelvin probe technique and AFM. Volta-potential difference that existed in the deformed microstructure and their misorientation was related. For this, the EBSD and SKPFEM together were used [29]. Further, the technique of EBSD has been used with other spectroscopic and microscopic techniques.

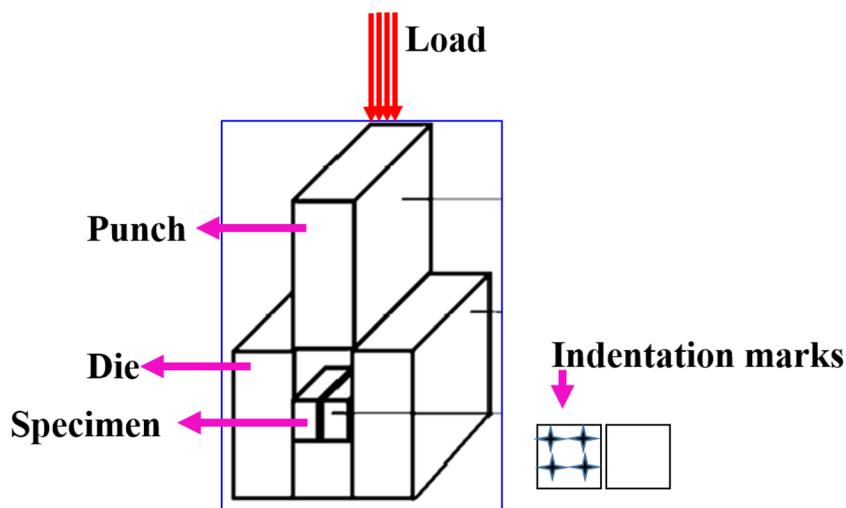
Experimental Methods

The alloy chemistry of austenitic stainless steel used in this study, varied, particularly chemical elements such as nickel, chromium, and molybdenum. The exact chemical composition of the alloy used in this study is shown in Table 1. To impose plastic strain of 0.58, these specimens were exactly machined and interrupted plastic deformation was carried out using a split-channel die plane compression test (SCDPCT) at room temperature (26 °C). The line diagram consists of die, punch, split specimens (Fig. 1) facilitated to assess information from same microstructural locations

between different measurement techniques (EBSD: for misorientation, potentiostat workstation using conventional three-electrode cell: for anodic polarization curve and FTIR-imaging: for Cr_2O_3 peak). The combination of SCDPCT and EBSD was used in this work for direct observation of deformed microstructures.

Indents were marked in the split specimens (Fig. 1) using the Vickers microhardness tester to facilitate for easy identification and location of the same microstructural regions. Details about the experimental methodology and procedure is found in this reference [30–32]. Further, this deformed specimen was given the heat treatment of 700 °C for 30 min, it was kept inside the furnace and the furnace was kept off and till it reaches the room temperature the complete duration and allowed to cool inside the furnace. The specimen prepared in this way hereinafter called heat-treated (HT) throughout this manuscript. Two different deaerated test solutions were used for recording anodic potentiodynamic polarization behavior. These were 0.5 M H_2SO_4 and 3 M HCl. The conventional three-electrode cells were used to record anodic potentiodynamic polarization behavior. The complete details including methodology, technical aspects of the anodic potentiodynamic polarization experiment, EBSD measurements and FTIR-imaging were provided in this reference [14, 33, 34]. The Bruker™ 300-Hyperion experimental setup was used to extract Cr_2O_3 peak at a wavenumber of 660 cm^{-1} approximately.

Fig. 1 Assembly of split-channel die plane compression test (SCDPCT) used in this study



Further, area under Cr_2O_3 peak was estimated using the post-processing FTIR-imaging OPUS 6.5™ software.

Results and Discussion

The plane strain compression (PSC) test using channel die split set up (Fig. 1) was enabled to observe the same microstructural regions. The stainless steel specimens were subjected to the true strain of 0.58 using SCDPCT technique. The typical anodic potentiodynamic polarization curve consists of three regions (active, passive and transpassive) for materials that exhibit passive materials (Fig. 2(a)). The anodic potentiodynamic polarization parameters (E_{crit} , i_{crit} , i_p) derived from its curve (Fig. 2(a)) are detailed in this reference [33]. The relevance and definition of E_{crit} , i_{crit} , and i_p are also detailed in this reference [33]. For instance, increase in i_{crit} and i_p indicated that difficulties in achieving passivity. The condition/state of surface finish, phases and microstructural features affect the anodic polarization parameters. The initiation of pit event is generally identified by spikes (potential vs current density plot) [35]. Hence, the ideal polarization curves of passivable metals and alloys exhibit such an absence of current spikes (Fig. 2(a)), when the test solution consists of

chlorides such current spikes are visible (Fig. 2(b)). Further, the absence of current spikes indicates the ease of passivity in the test solution of H_2SO_4 (Fig. 2(c)). According to Saadi et al. (2016), from the anodic potentiodynamic polarization curve, it is possible to differentiate clearly the events of pit initiation and formation of metastable pits [36]. In the deaerated test solution of 3 M HCl (very aggressive), achievement of the passivity was difficult for as received and deformed specimen (Fig. 2(c)), relatively better passivity was obtained after HT (Fig. 2(b)). Further, in the deaerated test solution of 0.5 H_2SO_4 better passivity was obtained in all specimens. The HT increases the corrosion resistance than the deformed specimens (true strain of 0.58) as clearly established through overall anodic polarization curve (Fig. 2(b)). The average grain sizes are determined for as-received state of Sanicro 28™, AISI316L, and AISI304L. These are 180 μm for Sanicro 28™, 15 μm for AISI316L and AISI304L respectively. The concept of grains in EBSD is slightly different. Based on the user-defined set grain tolerance angle (GTA), algorithm considers and assigns to the same grain. The imposed deformation reduced the grain size for all deformed specimens. The heat treatment of 700 °C 30 min slightly altered the grain size (Table 2). This is seen in all grades of austenitic stainless steel (Table 2). In general, the plastic deformation of austenitic stainless steels produces a

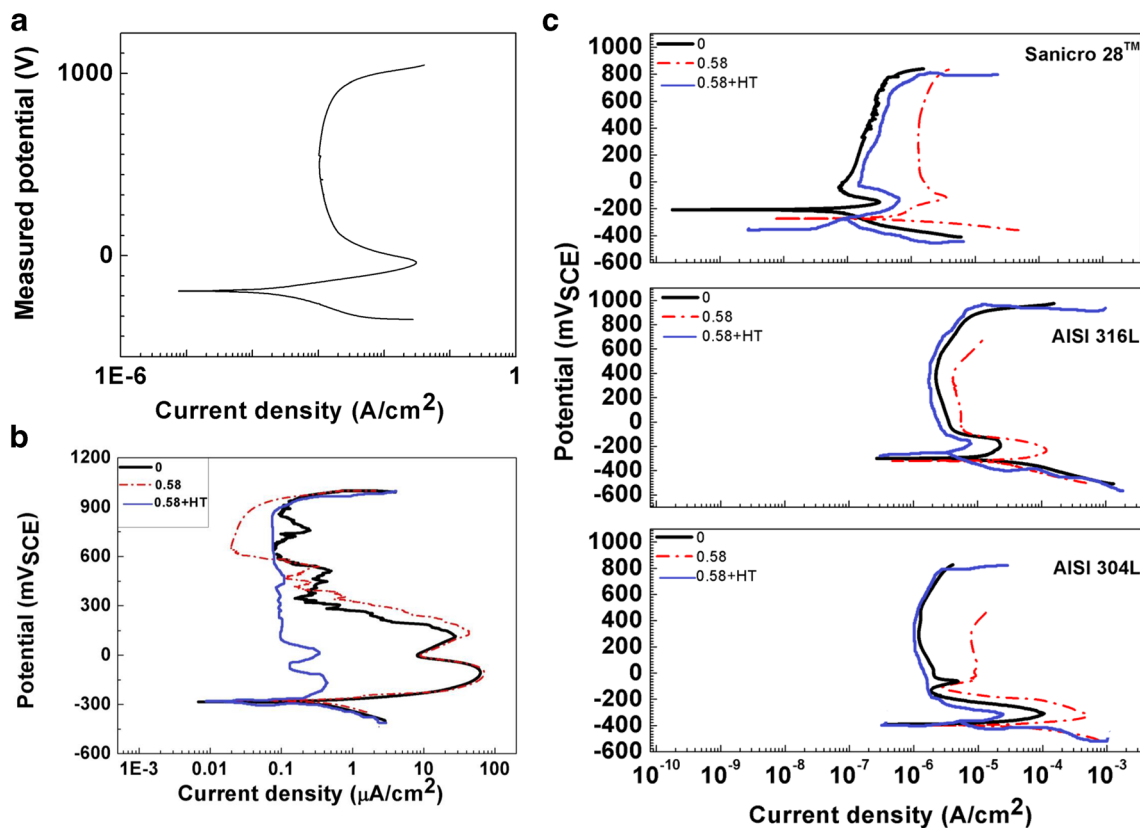


Fig. 2 (a) Schematic of anodic potentiodynamic polarization curve. (b) potentiodynamic anodic polarization curves of as-received, deformed and heat-treated specimens of Sanicro 28™ tested in deaerated solution (3 M

HCl) and (c) specimens of three grades tested in deaerated solution of 0.5 M H_2SO_4 . This anodic potentiodynamic polarization test was obtained using the potentiostat three-electrode setup

Table 2 Parameters as estimated from EBSD system

Materials		Sanicro 28™			AISI316L			AISI304L		
		ε=0	ε=0.58	0.58+HT	ε=0	ε=0.58	0.58+HT	ε=0	ε=0.58	0.58+HT
Parameters	Grain size(μm)	162±20	85±15	40±15	15±5	10±3	11±3	15±5	12±3	9±3
	GAM (°)	0.30	0.81	0.4	0.34	1.27	0.55	0.24	0.82	0.66
	KAM (°)	0.29	0.81	0.5	0.34	1.28	0.54	0.28	0.85	0.59
	GOS (°)	0.32	0.84	0.45	0.39	1.31	0.50	0.23	0.81	0.67

change in microstructural aspects. These range from change in grain aspect size to development of complex dislocation substructures and formation of new phases. It has been reported that influence of these microstructural changes affect the corrosion resistance of austenitic stainless steel. For instance, large body of published literature suggested that formation of new phases (strain-induced martensite) reduced the corrosion resistance in general [37] and further it has been argued that corrosion resistance depends on substrate microstructure (location dependent). The one of the present author has explored the significance of strain-induced martensite (SIM) in retaining stability of passive film [33]. Some disagreements/arguments exists about the role of SIM. These are extensively discussed in the references [15, 37–44]. The EBSD-IQ map revealed that (Fig. 3) signatures of plastic deformation. These are development of strain localization, lattice curvature, and slip lines/bands. The structural changes in metallic materials are related to properties. The EBSD is a powerful tool to visualize the crystal orientation, development of misorientation. The EBSD parameters describing misorientation parameters. In another study, it has been reported that the image quality (IQ) map has been used to assess the degree of sensitization (DOS) [45]. For instance, KAM has been used to understand the extreme local lattice distortions [46], and to characterize the stored energy, as this is driving force for recrystallization [47]. In another work, the value of grain orientation spread (GOS) was used to relate initiation of pitting in stainless steel [48–50]. It has been reported that the plastic strain is an influencing parameter that degrades the materials. Further the initiation of cracks and stress corrosion cracking (SCC) is accelerated by the presence of plastic strain. The 2-dimensional EBSD misorientation parameters such as grain

average misorientation (GAM), kernel average misorientation (KAM), grain orientation spread (GOS), image quality (IQ) maps [51] have been used to correlate with the degree of deformation and properties of the materials. This has become now standard practice of characterizing the deformed metallic materials. As IQ maps are directly related to lattice imperfection [52], many studies were reported to use as effective parameters. There exists a linear relationship between KAM and plastic strain is also observed in this study. This is in line with the literature [53]. The pattern region of interest analysis system (PRIAS™), is an emerging technology that is attached to an EBSD system, for capturing the microstructural features and distribution. In this study, the PRIAS™ techniques were used, to capture the pits morphology (Fig. 4). It is concluded that formation of pits was extremely random and stochastic in nature in aggressive test solution (3 M HCl). This behavior is observed in all grades of as-received specimens. Hence it was decided to make an attempt to identify the exact microstructural locations, were initiations of nucleation of pits. This remains challenging and unanswered due to multiple mechanism at play. The efforts have been made for finding models/mechanism addressed but however, it is extremely system specific. Further, it has been clearly established that the properties of the passive film depend on chemical composition, in turn depend on location of the microstructural defects.

The damage (destruction of passive film) arises from either chemical, mechanical or electrical. When this happens (breakdown of passive film), it leads to localized corrosion (pitting corrosion, crevice corrosion, stress corrosion cracking). In addition, alloy chemistry also plays a major role in retaining passivity. Various research reports have indicated that the

Table 3 Cr₂O₃ peak area as obtained from FTIR-imaging of all specimens

Materials	Sanicro 28™			AISI316L			AISI304L		
	ε=0	ε=0.58	0.58+HT	ε=0	ε=0.58	0.58+HT	ε=0	ε=0.58	0.58+HT
Condition of specimens	0.341	0.023	0.071	0.081	0.012	0.065	0.041	0.005	0.032

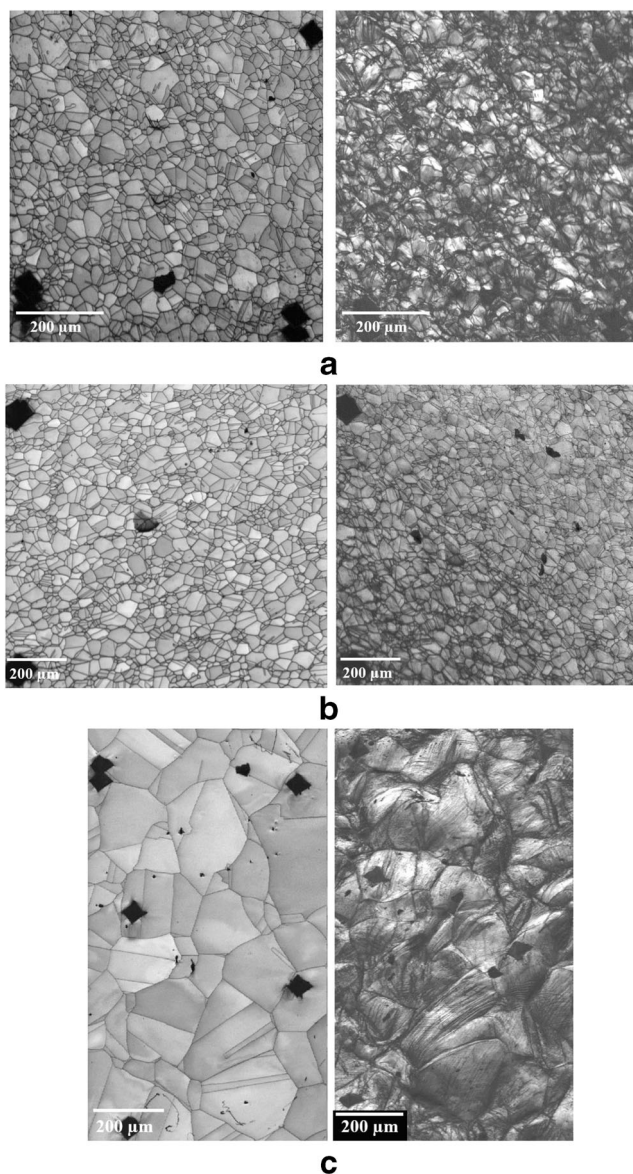


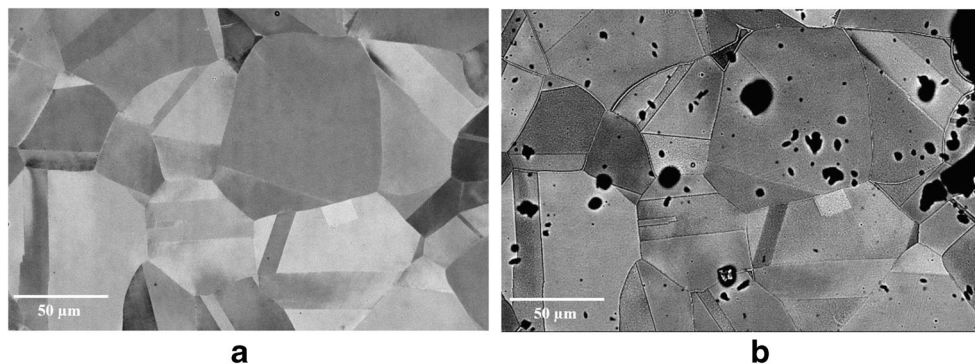
Fig. 3 IQ maps from EBSD of as-received and deformed specimen ($\epsilon=0.58$) of (a) AISI 304 L, (b) AISI 316 L and (c) Sanicro 28™

manganese sulfide in stainless steels initiates for passivity breakdown. It is known that, homogeneous (uniform, defect

free) system of passive film is not deteriorated. In another work, breakdown of passivity model has been proposed with grain boundaries taken into account [54]. Then, the experiment was designed to link the microstructural information with passivation by combination of EBSD +FTIR-imaging. Both techniques serve to complement each other. To implement this, the same area of microstructure was selected to examine by EBSD +FTIR-imaging techniques in this manuscript. In general, passivity breakdown refers to damage of passive film.

The perfect passive film without any defects, generally do not breakdown. Unfortunately such a system is of ideal in nature. The commercially available metals and alloys contain grain, grain boundaries, chemical element inhomogeneity. Further, the pores and micro-cracks also showed to affect the passive film and its stability. These acts as a potential site for passive film breakdown. In the past, large body of literature covering the aspects of pitting corrosion events such as nucleation, initiation, propagation, and metastable pits. These are detailed in this reference. The FTIR-imaging setup was used to record Cr_2O_3 peak approximately $650\text{--}660\text{ cm}^{-1}$ at the surface of the specimens. For passivable metals and alloys, the formation and stability of passive film is a key, and this is influenced by structural heterogeneities. U.R. Evans [55], he was the one who discussed pitting corrosion of metals, particularly iron. Challenges and disagreements do exist in this area of passivation, as complete understanding is still lagging, even with the advancement of science and technology. Transmission electron microscopy (TEM), and energy-dispersive X-ray spectroscopy (EDX) techniques have been used for direct evidence of passive film and nanoneedles were observed [56]. Step-like unevenness in passive film has also been observed at the grain boundary of duplex steels using aberration corrected TEM [18]. Time of flight secondary ion mass spectroscopy (ToF-SIMS), x-ray photoelectron spectroscopy (XPS) and scanning tunneling microscopy (STM) has been used to reveal the atomic structure of the passive film. These studies have confirmed that Cr content and

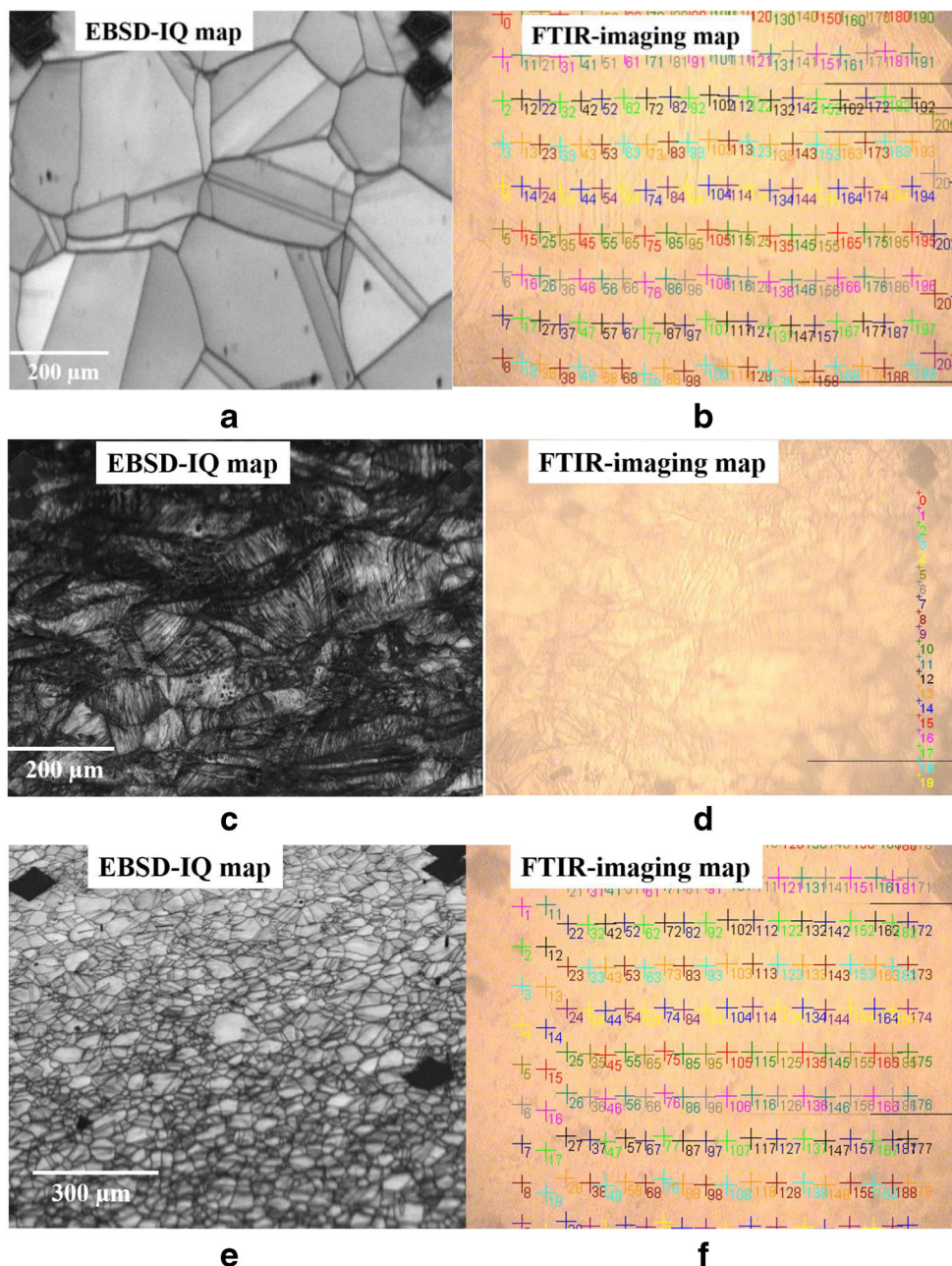
Fig. 4 PRIAS™ imaging from EBSD system for (a) as-received state of before and (b) after anodic polarization test of Sanicro 28™



polarization conditions have played a role in passivity. Further, the role of Mo on passivation has been detailed in terms of composition and morphology [57]. Others addressed the effect of local misorientations and pitting corrosion of pearlite steel. They have estimated that the EBSD parameters such as grain tolerance angle (GTA) and GOS and related to local passivation [49]. The regions that exhibited higher grain stored energy attacked earlier for Al alloys [58] and further that have reported that no relationship with grain misorientation and corrosion attack. Further, effect of GOS on pitting corrosion was investigated for duplex [48] and martensitic stainless

steels [50]. In another work, in situ measurements were performed using scanning tunneling microscopy (STM) and IR spectroscopy. Here, detailed microscopic and spectroscopic information was obtained for Cu specimens tested in HCl [59]. Thus, the possibilities of combined techniques such as advanced microscopic and spectroscopic techniques have yielded new-insights about the passive film. Hence, in this work, the experiment was designed to extract the information of passive film at different microstructural locations using EBSD and FTIR-imaging technique (Fig. 5). The average area of Cr₂O₃ extracted in this way was consolidated and presented

Fig. 5 The combined examination of EBSD+FTIR-imaging of (a-b) Sanicro 28™, (c-d) AISI 316 L, and (e-f) AISI 304 L materials



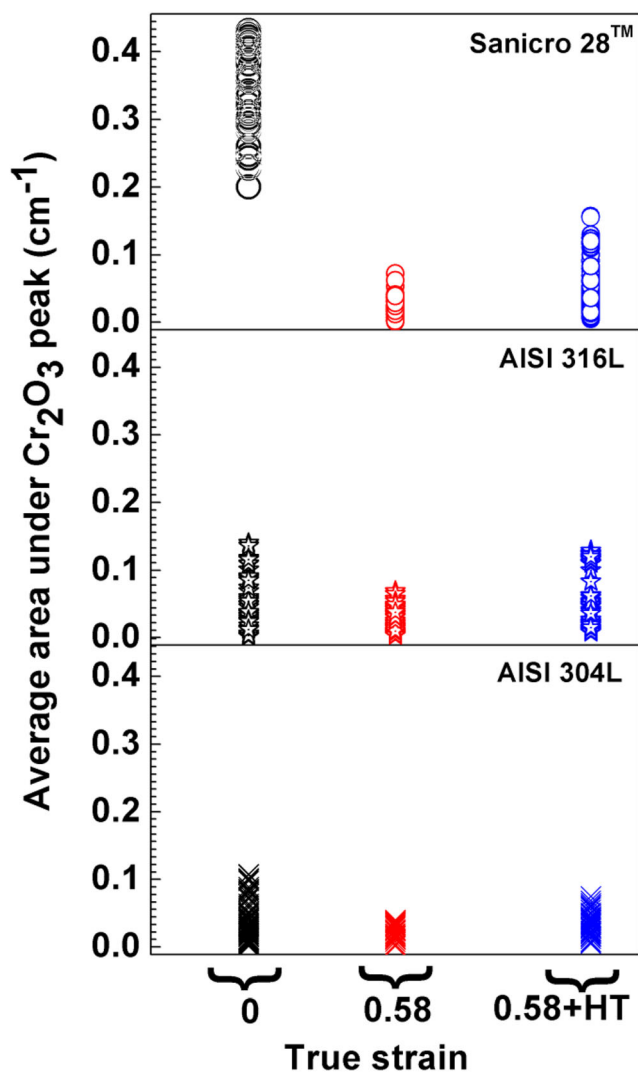


Fig. 6 The evolution of Cr₂O₃ peaks of as-received, deformed (true strain of 0.58) and HT specimens after potentiodynamic polarization test. The average value is reported from 100 such measurement

(Fig. 6), suggested that the as-received of Sanicro 28™ specimens (0.341) exhibited high compared to all other specimens. This is due to higher wt (%) of chromium present in this grade. The average value of all specimens as extracted from FTIR-imaging were presented in Table 3. The deformed specimens (true strain of 0.58) were exhibited lesser than as-received state. The slight improvement in average value after HT was noticed, however this improvement was equal to as-received specimens. At this juncture, it is important to correlate the relevant previous studies have carried out by one of present authors, [14, 33] have reported that strong presence of FTIR signal has indicated the possible role of SIMF as confirmed by EBSD measurements. In addition, the role of SIMF particles on deformed specimens, particularly on class of stainless steels has been explored widely and often results were contradictory [15, 37, 38]. In an recent

study, carefully isolated individual phase specific experiments were carried out and corrosion behavior was observed in super duplex stainless steel [60]

Conclusions

Three grades of stainless steel specimens were plastically deformed and imposed a true strain of 0.58 and these steels were given heat treatment of 700 °C for 30 min. Further, the anodic potentiodynamic polarization experiment was carried out for all specimens. It was noted that from the anodic potentiodynamic polarization curve that passivity was clearly established in specimens of as-received and 0.58+HT in deaerated 0.5 M H₂SO₄ test solution. The two anodic peaks and metastable current spikes were observed in the as-received and deformed (true strain of 0.58) specimens in deaerated 3 M HCl test solution. The formation and morphology of pits as captured by PRIAS™ revealed that independent of microstructural features and random. Further, when deformed specimens were given heat treatment of 700 °C for 30 min, such second anodic peaks and metastable current spikes were not observed. The FTIR-imaging was used to capture the Cr₂O₃ peaks and its average area was quantified. In the un-deformed state, the specimens of the average area were estimated as 0.34, 0.081 and 0.041 for Sanicro 28™, AISI 316 L, and AISI 304 L respectively. Further, deformed specimens to the tune-up to 0.58 true stain, the decrease was gradual as expected, and average area was lower than undeformed state. These were 0.023, 0.012 and 0.005 for Sanicro 28™, AISI 316 L, and AISI 304 L respectively. However, when these specimens were heat-treated, the slight improvement in average area was higher than the deformed. The combined multi-physics and multi-scale (atomic/nano) approaches are needed to unravel the exact cause of local (atomic/nano) corrosion mechanism. In essence, the simultaneous correlation of microstructural features with localized corrosion development in the way of well-thought and carefully designed experiment is needed.

Compliance with Ethical Standards

Conflict of Interest The author declare that no conflict of interest.

References

- Oh YJ, Hong JH (2000) Nitrogen effect on precipitation and sensitization in cold-worked type 316L(N) stainless steels. *J Nucl Mater* 278:242–250
- Jones R, Randle V, Owen G (2008) Carbide precipitation and grain boundary plane selection in overaged type 316 austenitic stainless steel. *Mater Sci Eng A* 496:256–261
- Hong S, Kim M, Min D, Lee K, Shim J, Kim D, Suh J, Jung W, Choi I (2014) Unraveling the origin of strain-induced precipitation

- of M 23 C 6 in the plastically deformed 347 austenite stainless steel. *Mater Charact* 94:7–13
4. Advani AH, Atteridge DG, Murr LE (1991) Solution annealing effects on sensitization of 316 stainless steels. *Scripta Metallurgica Mater* 25:2221–2226
 5. Pradhan SK, Prithiv TS, Mandal S (2017) Through-thickness microstructural evolution during grain boundary engineering type thermomechanical processing and its implication on sensitization behavior in austenitic stainless steel. *Mater Charact* 134:134–142
 6. Ghosh S, Kain V (2010) Effect of surface machining and cold working on the ambient temperature chloride stress corrosion cracking susceptibility of AISI 304L stainless steel. *Mater Sci Eng A* 527:679–683
 7. Kumar PS, Acharyya SG, Rao SVR, Kapoor K (2017) Distinguishing effect of buffing vs. grinding, milling and turning operations on the chloride induced SCC susceptibility of 304L austenitic stainless steel. *Mater Sci Eng A* 687:193–199
 8. Singh R, Chowdhury SG, Ravi Kumar B, Das SK, De PK, Chattoraj I (2007) The importance of grain size relative to grain boundary character on the sensitization of metastable austenitic stainless steel. *Scr Mater* 57:185–188. <https://doi.org/10.1016/j.scriptamat.2007.04.017>
 9. Farahat AIZ, El-Bitar TA (2010) Effect of Nb, Ti and cold deformation on microstructure and mechanical properties of austenitic stainless steels. *Mat Sci Eng A* 527:3662–3669
 10. Hamdy AS, El-Shenawy E, El-Bitar T (2007) The corrosion behavior of niobium bearing cold deformed austenitic stainless steels in 3.5% NaCl solution. *Mater Lett* 61:2827–2832
 11. Malki B, Le Bacq O, Pasturel A, Baroux B (2014) Ab initio study of water related defects in Cr₂O₃ and the consequences for the stability of passive films of stainless steels. *J Electrochem Soc* 161:486–493. <https://doi.org/10.1149/2.0701410jes>
 12. Taveira LV, Montemor MF, Da Cunha Belo M, Ferreira MG, Dick LFP (2010) Influence of incorporated Mo and Nb on the Mott-Schottky behaviour of anodic films formed on AISI 304L. *Corros Sci* 52:2813–2818
 13. Bai G, Lu S, Li D, Li Y (2016) Influences of niobium and solution treatment temperature on pitting corrosion behaviour of stabilised austenitic stainless steels. *Corros Sci* 108:111–124. <https://doi.org/10.1016/j.corsci.2016.03.009>
 14. Srinivasan N, Senthil Kumaran S (2019) Role of alloy chemistry on stability of passive films in austenitic stainless steel grades. *J Mater Eng Perform* 28:3695–3703
 15. Peguet L, Malki B, Baroux B (2007) Influence of cold working on the pitting corrosion resistance of stainless steels. *Corros Sci* 49:1933–1948
 16. Zhang B, Wang J, Wu B, Guo XW, Wang YJ, Chen D, Zhang YC, Du K, Oguzie EE, Ma XL (2018) Unmasking chloride attack on the passive film of metals. *Nat Commun* 9:1–9. <https://doi.org/10.1038/s41467-018-04942-x>
 17. Ogunsanya IG, Hansson CM (2019) The semiconductor properties of passive films and corrosion behavior of stainless steel reinforcing bars in simulated concrete pore solution. *Materialia* 6:100321. <https://doi.org/10.1016/j.mtla.2019.100321>
 18. Zhang B, Wei XX, Wu B, Wang J, Shao XH, Yang LX, Zheng SJ, Zhou YT, Jin QQ, Oguzie EE, Ma XL (2019) Chloride attack on the passive film of duplex alloy. *Corros Sci* 154:123–128. <https://doi.org/10.1016/j.corsci.2019.04.012>
 19. Massoud T, Maurice V, Klein LH, Seyeux A, Marcus P (2014) Nanostructure and local properties of oxide layers grown on stainless steel in simulated pressurized water reactor environment. *Corros Sci* 84:198–203. <https://doi.org/10.1016/j.corsci.2014.03.030>
 20. Jinlong L, Tongxiang L, Chen W, Limin D (2015) Comparison of corrosion properties of passive films formed on coarse grained and ultrafine grained AISI 2205 duplex stainless steels. *J Electroanal Chem* 757:263–269. <https://doi.org/10.1016/j.jelechem.2015.09.036>
 21. Jinlong L, Hongyun L (2013) Comparison of corrosion properties of passive films formed on phase reversion induced nano/ultrafine-grained 321 stainless steel. *Appl Surf Sci* 280:124–131
 22. Jinlong L, Tongxiang L, Chen W, Ting G (2016) Effect of in site strain on passivated property of the 316L stainless steels. *Mater Sci Eng C* 61:32–36. <https://doi.org/10.1016/j.msec.2015.12.010>
 23. Jinlong L, Hongyun L (2012) Electrochemical investigation of passive film in pre-deformation AISI 304 stainless steels. *Appl Surf Sci* 263:29–37
 24. Phadnis SV, Satpati AK, Muthe KP, Vyas JC, Sundaresan RI (2003) Comparison of rolled and heat treated SS304 in chloride solution using electrochemical and XPS techniques. *Corros Sci* 45:2467–2483
 25. Rangel CM, Silva TM, Belo M d C (2005) Semiconductor electrochemistry approach to passivity and stress corrosion cracking susceptibility of stainless steels. *Electrochim Acta* 50:5076–5082
 26. Gaffney JS, Marley NA, Jones DE (2012) Fourier transform infrared (FTIR) spectroscopy. In: Kaufmann EN (ed) *Charact Mater*. John Wiley & Sons, Ltd, pp 1104–1135
 27. Wang M, Zhou Z, Wang Q, Wang Z, Zhang X, Liu Y (2019) Role of passive film in dominating the electrochemical corrosion behavior of FeCrMoCBy amorphous coating. *J Alloys Compd* 811:151962. <https://doi.org/10.1016/j.jallcom.2019.151962>
 28. Ömek C, Leygraf C, Pan J (2019) Author correction: passive film characterisation of duplex stainless steel using scanning kelvin probe force microscopy in combination with electrochemical measurements. *Npj Mater Degrad* 3:1–8. <https://doi.org/10.1038/s41529-019-0077-2>
 29. Ömek C, Engelberg DL (2015) SKPFM measured Volta potential correlated with strain localisation in microstructure to understand corrosion susceptibility of cold-rolled grade 2205 duplex stainless steel. *Corros Sci*:4–11
 30. Panchanadeeswaran S, Doherty RD, Becker R (1996) Direct observation of orientation change by channel die compression of polycrystalline aluminum - use of a split sample. *Acta Mater* 44:1233–1262
 31. Srinivasan N, Kain V, Samajdar I, Krishna KVM, Sivaprasad PV (2017) Plane strain compression testing of Sanicro 28 by channel-die compression test: a direct microstructural observation. *Mater Today Proc* 4:9888–9892
 32. Chappelle D, Darrieulat M (2003) The occurrence of shear banding in a millimeter scale (1̄23)[634] grain of an Al-4.5% mg alloy during plane strain compression. *Mater Sci Eng A* 347:32–41. [https://doi.org/10.1016/S0921-5093\(02\)00556-7](https://doi.org/10.1016/S0921-5093(02)00556-7)
 33. Srinivasan N, Kain V, Birbilis N, Kumar BS, Gandhi MN, Sivaprasad PV, Chai G, Lodh A, Ahmedabadi PM, Samajdar I (2016) Plastic deformation and corrosion in austenitic stainless steel: a novel approach through microtexture and infrared spectroscopy. *Corros Sci* 111:404–413
 34. Srinivasan N, Kumaran SS, Venkateswarlu D (2018) Effects of plastic strains on passivation behavior of different austenitic stainless steel grades. *Mater Res Express* 6:026504. <https://doi.org/10.1088/2053-1591/aaea2d>
 35. Wells DB, Williams DE (1991) Initiation events for pitting corrosion of stainless steel. *Corr Sci* 32:1307–1313
 36. Al Saadi S, Yi Y, Cho P, Jang C, Beeley P (2016) Passivity breakdown of 316L stainless steel during potentiodynamic polarization in NaCl solution. *Corros Sci* 111:720–727
 37. Elayaperumal K, De PK, Balachandra J (1972) Passivity of type 304 stainless steel—effect of plastic deformation. *Corrosion* 28:269–273
 38. Alvarez SM, Bautista A, Velasco F (2013) Influence of strain-induced martensite in the anodic dissolution of austenitic stainless steels in acid medium. *Corros Sci* 69:130–138

39. Srinivasan NR, Bandyopadhyaya R (2016) $\text{Sn}_x\text{Ti}_{1-x}\text{O}_2$ solid-solution-nanoparticle embedded mesoporous silica (SBA-15) hybrid as an engineered photocatalyst with enhanced activity. *Faraday Discuss* 186. <https://doi.org/10.1039/c5fd00126a>
40. Hamada AS, Karjalainen LP, Somani MC (2006) Electrochemical corrosion behaviour of a novel submicron-grained austenitic stainless steel in an acidic NaCl solution. *MatSciEng A* 431:211–217
41. Peguet L, Malki B, Baroux B (2009) Effect of austenite stability on the pitting corrosion resistance of cold worked stainless steels. *Corros Sci* 51:493–498
42. Barbucci A, Delucchi M, Panizza M, Sacco M, Cerisola G (2001) Electrochemical and corrosion behaviour of cold rolled AISI 301 in 1 M H_2SO_4 . *J Alloys Compd* 317–318:607–611
43. Barbucci A, Cerisola G, Cabot PL (2002) Effect of cold-working in the passive behavior of 304 stainless steel in sulfate media. *J Electrochem Soc* 149:B534–B542
44. LvJinlong L (2014) Hongyun, effects of strain and strain-induced α' -martensite on passive films in AISI 304 austenitic stainless steel. *Mater Sci Eng C* 34:484–490
45. Jinlong L, Zhuqing W (2019) Sensitization evaluation of the AISI 2205 duplex stainless steel by the IQ value in EBSD technique. *Eng Fail Anal* 105:65–69. <https://doi.org/10.1016/J.ENGFAILANAL.2019.07.001>
46. Saraf L (2011) Kernel average misorientation confidence index correlation from FIB sliced Ni-Fe-Cr alloy surface. *Microsc Microanal* 17:424–425
47. Tanure L, Bakaeva A, Dubinko A, Terentyev D, Verbeken K (2019) Effect of annealing on microstructure, texture and hardness of ITER-specification tungsten analyzed by EBSD, vickers microhardness and nano-indentation techniques. *J Nucl Mater* 524:191–199. <https://doi.org/10.1016/j.jnucmat.2019.07.005>
48. Vignal V, Ba D, Zhang H, Herbst F, Le Manchet S (2013) Influence of the grain orientation spread on the pitting corrosion resistance of duplex stainless steels using electron backscatter diffraction and critical pitting temperature test at the microscale. *Corros Sci* 68:275–278
49. Rault V, Vignal V, Krawiec H, Dufour F (2015) Quantitative assessment of local misorientations and pitting corrosion behaviour of pearlitic steel using electron backscattered diffraction and microcapillary techniques. *Corros Sci* 100:667–671
50. Vignal V, Ringeval S, Thiébaud S, Tabalaiev K, Dessolin C, Heintz O, Herbst F, Chassagnon R (2014) Influence of the microstructure on the corrosion behaviour of low-carbon martensitic stainless steel after tempering treatment. *Corros Sci* 85:42–51
51. Wu J, Wray PJ, Garcia CI, Hua M, Deardo AJ (2005) Image quality analysis: a new method of characterizing microstructures. *ISIJ Int* 45:254–262
52. Schwarzer RA, Field DP, Adams BL, Kumar M, Schwartz AJ (2009) Present state of electron backscatter diffraction and prospective developments. In: Schwartz AJ, Kumar M, Adams BL, Field DP (eds) *Electron backscatter Diffr. Mater. Sci.* Springer Science + Business media, New York, pp 1–20
53. Gussev MN, Edmondson PD, Leonard KJ (2018) Beam current effect as a potential challenge in SEM-EBSD in situ tensile testing. *Mater Charact* 146:25–34. <https://doi.org/10.1016/j.matchar.2018.09.037>
54. Marcus P, Maurice V, Strehblow HH (2008) Localized corrosion (pitting): a model of passivity breakdown including the role of the oxide layer nanostructure. *Corros Sci* 50:2698–2704. <https://doi.org/10.1016/j.corsci.2008.06.047>
55. EVANS U (1927) The passivity of metals. Part I. the isolation of the protective film. *J Chem Soc*:1020–1040
56. Zhang B, Hao S, Wu J, Li X, Li C, Di X, Huang Y (2017) Direct evidence of passive film growth on 316 stainless steel in alkaline solution. *Mater Charact.* <https://doi.org/10.1016/j.matchar.2017.05.013>
57. Maurice V, Peng H, Klein LH, Seyeux A, Zanna S, Marcus P (2015) Effects of molybdenum on the composition and nanoscale morphology of passivated austenitic stainless steel surfaces. *Faraday Discuss* 180:151–170
58. Luo C, Zhou X, Thompson GE, Hughes AE (2012) Observations of intergranular corrosion in AA2024-T351: the influence of grain stored energy. *Corros Sci* 61:35–44. <https://doi.org/10.1016/j.corsci.2012.04.005>
59. Vogt MR, Nichols RJ, Magnussen OM, Behm RJ (1998) Benzotriazole adsorption and inhibition of Cu(100) corrosion in HCl: a combined in situ STM and in situ FTIR spectroscopy study. *J Phys Chem B* 102:5859–5865
60. Mondal R, Bonagani SK, Lodh A, Sharma T, Sivaprasad PV, Chai G, Kain V, Samajdar I (2019) Relating general and phase specific corrosion in a super duplex stainless steel with phase specific microstructure evolution. *Corrosion* 75:1315–1326. <https://doi.org/10.5006/3091>

Publisher's Note Springer Nature remains neutral with regard to jurisdictional claims in published maps and institutional affiliations.

